JACS
JOURNAL OF THE AMERICAN CHEMICAL SOCIETY
pubs.acs.org/JACS

Article

$Eu_2Li(C_3)H$: A Carbide Hydride Phase Incorporating Eu^{2+}

Tim Kleinöder, Carolin Hoverath, Thomas Lorenz, Joshua Wiethölter, Theresa Block, Rainer Pöttgen, Tom Förster, Markus Suta, and Uwe Ruschewitz*

Cite This: https://doi.org/10.1021/jacs.5c19173

Read Online

ACCESS | Metrics & More | Article Recommendations | Supporting Information

ABSTRACT: Reactions between carbon and lithium hydride in a mixed metal europium/lithium flux led to the synthesis of $Eu_2Li(C_3)H$. At room temperature, the compound crystallizes in the tetragonal space group $P4/mbm$ (no. 127, $Z = 2$; $Ca_2Li(C_3)H$ type) and undergoes a second-order structural phase transition below ~250 K to an orthorhombic low-temperature modification (no. 55, $Pbam$; $Z = 4$), crystallizing in a new structure type. The phase transition was monitored by using single-crystal X-ray diffraction (SCXRD) and temperature-dependent high-resolution powder diffraction data. Infrared (IR) spectroscopy and gaschromatographic analysis (GC) of the hydrolysis products confirm the existence of a first europium compound with an allylenide anion (C_3^{4-}). Magnetic susceptibility measurements and ^{151}Eu Mössbauer spectroscopy reveal the presence of divalent europium, suggesting a charge-balanced carbide hydride $(Eu^{2+})_2(Li^+)(C_3^{4-})(H^-)$. A transition to a (soft) ferromagnetic ground state is observed below 42 K. *In situ* high-pressure, high-temperature (HPHT) investigations indicate a surprisingly high stability of $Eu_2Li(C_3)H$ and yield a bulk modulus $K_0 = 65$ GPa. Quantum chemical calculations (DFT + U) reveal a pseudogap at the Fermi level and allow the classification as a rare-earth metal Zintl phase exhibiting both ionic and covalent bonding contributions.

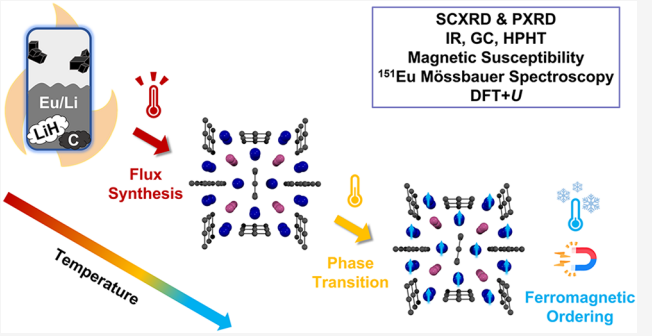

INTRODUCTION

Carbides are an intriguing class of compounds, due to the intermediate electronegativity (EN) of carbon (EN = 2.55 according to Pauling[1]), compounds with a more covalent or ionic bonding character may be found depending on the electronegativity of the respective bonding partner.[2] For example, in SiC (EN(Si) = 1.90) or $B_4C/B_{13}C_2$ (EN(B) = 2.04), strong covalent bonds are formed, leading to extremely hard materials being used as ceramics.[3] On the other hand, with elements of low electronegativity like alkali and alkaline earth metals, typically salt-like carbides are found with C^{4-} (methanides), C_2^{2-} (acetylides), or C_3^{4-} anions (allylenides).[2] With metals having a less electropositive character, typically a third, less well-defined class of metallic carbides was introduced with Fe_3C (important in the production of steel)[4] or WC (used in the tip of ballpoint pens)[5] being two prominent examples. Carbides of rare-earth elements (RE) are also attributed to this class of metallic carbides. There is a rich variety of possible compositions starting from RE_2C with RE/C = 2:1 and ending up with REC_2 (RE/C = 1:2).[6] Especially on the carbon-rich side, intriguing compounds with the compositions RE_4C_5, "$RE_{15}C_{19}$" (most likely identical to RE_3C_4), RE_3C_4, RE_2C_3 (better written as $RE_4(C_2)_3$), RE_4C_7, and REC_2 have been reported. In their crystal structures, isolated C_1 carbon atoms, but also C_2 and C_3 dumbbells as well as mixtures of these carbon moieties are found. All these compounds show metallic properties, i.e., metallic conductivity and metallic luster. There is only one exception: EuC_2! This compound is black and a semiconductor.[7] It contains Eu^{2+} and crystallizes in the monoclinic ThC_2-type structure ($C2/c$, no. 15, $Z = 4$) in contrast to all other REC_2 compounds, which crystallize in the tetragonal CaC_2–I type structure ($I4/mmm$, no. 139, $Z = 2$) and contain trivalent RE^{3+} cations. Another notable exception is YbC_2, for which an intermediate Yb valence of ~2.8 was reported based on various methods.[8−10] Obviously, europium (and ytterbium) carbides show specific properties, which makes them unique among the many examples of rare-earth metal carbides. This specific behavior of EuC_2 and YbC_2 can clearly be correlated to half (Eu^{2+}) and completely filled (Yb^{2+}) 4*f* valence shells. Unfortunately, with respect to europium carbides, EuC_2 is the only binary compound reported to date, and no compound crystallizing in the Pu_2C_3 type structure ($I\bar{4}3d$, no. 220, $Z = 8$), ubiquitous for all other rare-earth elements, has been reported for europium. EuC_6 is an intercalation compound and cannot be

Received: October 29, 2025
Revised: December 19, 2025
Accepted: December 23, 2025

considered a carbide.[11] Among the ternary compounds, $Eu_{3.16}NiC_6$ is of some interest, as the authors assumed a divalent state for europium in this material,[12] which was, however, not investigated further. $EuRh_3C$ is a metallic carbide with a perovskite-type structure. Compared to the other lanthanide (Ln) compounds $LnRh_3C$ of this series, no unusual behavior was reported for Ln = Eu.[13] In summary, europium carbides promise very interesting and unique properties, but their chemistry is not very well developed at the moment.

EuC_2 was synthesized from elemental europium and purified graphite at 1400 °C under inert conditions.[7] The product was obtained in the form of a black powder. In 2010, Latturner and co-workers used a metal flux approach to synthesize $Ca_2Li(C_3)H$ from calcium, lithium, carbon, and CaH_2.[14] Calcium and lithium were used in a surplus, thus forming the flux. The reaction temperature was in the range of 1050 to 500 °C to grow single crystals of the product. The approach to use metal flux for obtaining single crystals of carbides was also shown in a review from 2014, in which the synthesis of large single crystals of Li_2C_2 was presented.[15] The Latturner group was very successful with this approach and synthesized numerous carbides from metal fluxes beyond $Ca_2Li(C_3)H$, e.g., $La_{11}(MnC_6)_3$,[16] $Ca_{11}E_3C_8$ (E = Sn, Pb),[17] $Ca_{12}InC_{13-x}$,[18] $La_{15}(FeC_6)_4H$,[19] $LaCH_x$,[20] and La_3MC_2 (M = Sb, Bi, Te).[21]

However, despite several successful reports to incorporate lanthanide cations in their products, no successful synthesis of a europium-containing carbide was reported by the Latturner group to date, although the synthesis of europium compounds without carbon turned out to be successful using metal flux syntheses, e.g., as reported for the intermetallic phase EuMgSn.[22] It is notable that already in 1996 $Eu_{3.16}NiC_6$ (*vide supra*) was synthesized in a Li flux.[12] However, this successful approach was not pursued further.

In the following sections, we present the successful synthesis of a europium-containing carbide, namely, $Eu_2Li(C_3)H$, using metal fluxes. This compound is isostructural to $Ca_2Li(C_3)H$[14] at room temperature ($P4/mbm$, no. 127, $Z = 2$) but undergoes a structural phase transition at lower temperatures. This phase transition as well as some properties of $Eu_2Li(C_3)H$ will be described in detail.

EXPERIMENTAL SECTION

Synthesis

Single crystals of $Eu_2Li(C_3)H$ (Figure S1, Supporting Information) were obtained by reactions in a Eu/Li flux. In a typical experiment, a stainless-steel tube (6 cm length, 0.8 cm outer diameter, and 0.7 cm inner diameter) that was clamped and welded shut on one side was filled inside a glovebox with 3.3 mmol of europium (99.99%, smart elements, dendritic pieces), 2.5 mmol of lithium (99%, Merck), 1.8 mmol of carbon black (99%, abcr), and 0.67 mmol of lithium hydride (n/a) (argon atmosphere) in a molar ratio of 10:7.7:5.5:2. Alternatively, anthracene was added as a hydrogen source instead of lithium hydride. The ampules were arc-welded under argon and subsequently sealed in an evacuated silica tube. These ampules were heated in a vertical tube furnace to a temperature of 1323 K within 5 h, at which they were held for 2 h. The furnace was then cooled to 1073 K over 24 h before the temperature was further lowered to 773 K within 108 h. At 773 K, the ampules were quickly removed from the furnace, inverted, and centrifuged at 3500 rpm for 3 min. This allowed the excess Eu/Li flux to be removed from the crystals. $Eu_2Li(C_3)H$ can also be obtained from a stoichiometric reaction using the same temperature profile, but in this case, larger amounts of EuC_2 are produced as a byproduct. $Eu_2Li(C_3)H$ was obtained as black, lustrous, cuboid crystals (Figure S1), which are highly sensitive to air and moisture. In order to exclude any iron-containing impurities for the measurement of magnetic susceptibilities, the compound was synthesized in a tantalum ampule (instead of a stainless-steel ampule).

Single crystals of EuH_2 were synthesized from a Eu/Na flux with carbon black and anthracene (molar ratio: 10:9.2:3.1:0.2). Compared to the previously mentioned synthesis procedure, only the temperature program was (slightly) changed: the sample was heated to 1323 K in 5 h, kept at 1323 K for 2 h, cooled to 1173 K in 30 h, and further cooled to 1023 K in 75 h, followed by centrifugation.

Single-Crystal Structure Analysis

Single-crystal diffraction data were collected at 270(2) K for RT-, 240(2) K for LT-$Eu_2Li(C_3)H$, and 100 K for EuH_2 on a Bruker D8 venture diffractometer (Mo−Kα radiation, mirror-monochromator, λ = 0.71073 Å). A suitable crystal of $Eu_2Li(C_3)H$ was selected under a microscope in inert oil and quickly mounted under a N_2 stream on the diffractometer. The temperature of the measurement was controlled with an Oxford Cryostream 800 system. The data reduction and correction for absorption were carried out using SAINT[23] and SADABS[24] inside the APEX5[25] program package. A numerical absorption correction was applied for $Eu_2Li(C_3)H$, while a multiscan correction was used for EuH_2. An initial model was obtained with SHELXT[26] and was subsequently refined using SHELXL.[27] The difference Fourier maps were calculated using SHELXL[27] and visualized in ShelXle.[28] At the end of the structure refinement of RT-$Eu_2Li(C_3)H$ without assigning the hydrogen atom, a residual electron density peak (1.29 e/Å^3) was located on Wyckoff site 2*b* (Figure S2, Supporting Information). This residual electron density peak was observed in several measured crystals. In agreement with $Ca_2Li(C_3)H$, a hydrogen atom was refined isotropically on this site. Similarly, when the LT modification was refined, the highest residual electron density peak (1.07 e/Å^3) in the final refinement steps was assigned to a hydrogen atom. Further information concerning the refinements and selected structural data can be found in Tables 1 and 2 in the main body of the paper as well as Tables S1 and S5 (Supporting Information).

Table 1. Selected Crystallographic Data and Details of the X-ray Single-Crystal Structure Analysis of RT- and LT-$Eu_2Li(C_3)H$

	RT-$Eu_2Li(C_3)H$	LT-$Eu_2Li(C_3)H$
space group (number), Z	$P4/mbm$ (127), 2	$Pbam$ (55), 4
temperature [K]	270(2)	240(2)
a [Å]	7.1046(4)	10.0463(6)
b [Å]	= a	10.0553(6)
c [Å]	3.9335(4)	3.9340(3)
V [Å^3]	198.54(3)	397.41(5)
2θ range [°] (resolution)	8.11 to 60.80 (0.70 Å)	4.05 to 60.99 (0.70 Å)
radiation	Mo Kα	Mo Kα
reflections collected	4732	10136
independent reflections	189	689
	R_{int} = 0.0657	R_{int} = 0.0582
	R_{sigma} = 0.0221	R_{sigma} = 0.0276
data/restraints/parameters	189/0/16	689/0/44
goodness-of-fit on F^2	1.191	1.153
final R indexes [$I \geq 2\sigma(I)$]	R_1 = 0.0186	R_1 = 0.0207
	wR_2 = 0.0417	wR_2 = 0.0484
final R indexes [all data]	R_1 = 0.0189	R_1 = 0.0229
	wR_2 = 0.0418	wR_2 = 0.0490
largest peak/hole [e Å^{-3}]	1.12/−1.82	1.00/−1.36
TWIN	/	010 100 00−1
BASF	/	0.139(4)
deposition number	CSD-2488130	CSD-2488131

https://doi.org/10.1021/jacs.5c19173
J. Am. Chem. Soc. XXXX, XXX, XXX−XXX

Table 2. Selected Interatomic Distances (Å) in $Eu_2Li(C_3)H$[a]

	RT-$Eu_2Li(C_3)H$	LT-$Eu_2Li(C_3)H$	
	sc (270(2) K)	sc (240(2) K)	p (100(2) K)
Eu−H	Eu−H	Eu1−H	
	2.6047(2) 8x	2.59(3) 4x	2.617(2)[b] 4x
		2.62(3) 4x	2.591(2)[b] 4x
		Eu2−H	
		2.60(3) 4x	2.6704(9)[b] 4x
		2.62(3) 4x	2.5634(9)[b] 4x
Li−H	1.9668(2) 4x	1.969(1) 8x	1.980(3)[b] 8x
Eu−C	Eu−C1	Eu2−C1	
	2.6814(2) 8x	2.6816(2) 8x	2.6791(4) 8x
	Eu−C2	Eu1−C3	
	2.716(3) 8x	2.727(4) 8x	2.729(3) 8x
	2.992(3) 16x	Eu2−C3	
		2.967(4) 8x	2.920(10) 8x
		3.007(4) 8x	3.067(11) 8x
		Eu1−C2	
		2.6828(2) 8x	2.6873(4) 8x
		Eu2−C4	
		2.718(4) 8x	2.711(3) 8x
		Eu1−C4	
		2.977(3) 8x	2.983(12) 8x
		3.009(3) 8x	3.016(12) 8x
Li−C	Li−C2	Li−C3	
	2.777(4) 8x	2.655(10) 4x	2.50(4) 4x
		2.913(10) 4x	3.08(4) 4x
		Li−C4	
		2.639(9) 4x	2.49(3) 4x
		2.923(9) 4x	3.09(3) 4x
C−C	C1−C2	C1−C3	
	1.328(4) 4x	1.317(6) 4x	1.337(5)[c] 4x
		C2−C4	
		1.327(5) 4x	1.334(4)[c] 4x

[a](sc: single crystal; p: powder). [b]H position was constrained to the value of the sc measurement (240 K). [c]Distance restrain of 1.33(2) Å.

Powder X-ray Diffraction (PXRD)

PXRD data were collected at room temperature on a Stoe Stadi P powder diffractometer (Mo−Kα_1 radiation, Ge(111) monochromator, Mythen detector). Samples were measured in sealed glass capillaries (Ø = 0.2 mm, argon atmosphere). Typical acquisition times were 30 min. The WinXPow software package[29] was used for data handling, simulation of theoretical patterns, and visualization of the PXRD patterns.

Synchrotron Powder Diffraction

High-resolution synchrotron powder diffraction data were measured at beamline BL09 of the Center for Synchrotron Radiation (DELTA, Dortmund/Germany).[30] The radiation was adjusted to the desired wavelength of λ = 0.4592 Å using a silicon (311) double-crystal monochromator. The diffractometer is equipped with a PILATUS 100 K detector, and the photon source consists of a superconducting asymmetric wiggler (SAW2). For the experiments, samples were filled in glass capillaries (Ø = 0.2 mm) and sealed in an argon atmosphere. The capillaries were mounted horizontally on a spinning goniometer. Data were collected at room temperature and during cooling at 20 K intervals from 280 to 100 K. The temperature was controlled with an Oxford Cryostream 700 system.

Powder Diffraction: Data Evaluation

For the analysis of the temperature-dependent structural transformation, the measured synchroton powder diffraction data were evaluated using Rietveld refinements with the TOPAS 5 software.[31] The lattice parameters and atomic positions derived from the single-crystal structure analysis served as the starting model for the refinement of the RT and LT modifications of $Eu_2Li(C_3)H$. The unit cells and peak profiles were refined by using Pawley fits before the subsequent Rietveld refinements. A distance restrain of 1.33(2) Å was used for the C−C bond within the allylenide anion in the LT modification. In the final refinement cycles, all atoms were refined with isotropic displacement parameters (U_{iso}), but the U_{iso} values of the carbon atoms and hydrogen atoms were constrained to one common value in the RT modification. In the LT modification, the U_{iso} of the lithium atoms was additionally restricted to the same value, and the location of the hydrogen atom was fixed at the position derived from the low-temperature single-crystal structure analysis.

An exemplary Rietveld fit for the RT modification (ambient conditions) is depicted in Figure S3 and for the LT modification in Figure S4 (100 K; Supporting Information). Selected details of the Rietveld refinement and measurement of the synchrotron powder diffraction data at ambient conditions and 100 K are summarized in Table S6 (Supporting Information). Selected interatomic distances are given in Tables 2 and S5, and the atomic positional parameters are listed in Table S7 (Supporting Information).

CSD-2488130 ($Eu_2Li(C_3)H$, 270 K, single crystal), CSD-2488131 ($Eu_2Li(C_3)H$, 240 K, single crystal), CSD-2488132 ($Eu_2Li(C_3)H$, 100 K, powder), and CSD-2488135 (EuH_2, 100 K, single crystal) contain the supplementary crystallographic data for this paper. These data can be obtained free of charge via www.ccdc.cam.ac.uk/data_request/cif, or by emailing data_request@ccdc.cam.ac.uk, or by contacting The Cambridge Crystallographic Data Centre, 12 Union Road, Cambridge CB2 1EZ, U.K.; fax: + 44 1223 336033. Diamond, version 4.6.8 was used to visualize the crystal structures.[32]

Protolysis Study

To analyze the gas phase of $Eu_2Li(C_3)H$ after hydrolysis, a home-built gas chromatograph was used.[33] For the measurement, several single crystals of $Eu_2Li(C_3)H$ were quickly transferred to a small test tube in air without using inert conditions (e.g., argon atmosphere) as this gas may influence the results of the GC measurement. The test tube was promptly sealed with a septum, and 1 mL of water was added to the crystals using a syringe. After approximately 5 min, 3 mL of the evolved gas was removed using a second syringe and inserted into the GC. The hydrolysis products of Mg_2C_3[34] and LiH[35] were used as references.

IR Spectroscopy

IR spectra were recorded with a Bruker α FT-IR spectrometer using the ATR sample technique (with a diamond ATR crystal). The spectrometer was housed in a glovebox (argon atmosphere) to provide inert conditions.

Magnetic Susceptibilities

Several randomly oriented single crystals of $Eu_2Li(C_3)H$ (10.5 mg), synthesized in a tantalum ampule (vide supra), were sealed in a silica glass capillary (Ø = 2.0 mm; argon atmosphere). The magnetic susceptibilities were measured in a SQUID magnetometer (MPMS, Quantum Design) in the temperature range 2−300 K at a magnetic field of B_0 = 0.1 T. The field-dependent magnetization was recorded at 1.9 K in an external field ranging from −2 to +7 T. The diamagnetic contribution of $Eu_2Li(C_3)H$ was calculated to $\chi_m^{dia} = -27.5 \times 10^{-6}$ emu mol_{Eu}^{-1} according to the procedures described in the literature.[36]

^{151}Eu Mössbauer Spectroscopy

The ^{151}Eu Mössbauer spectroscopic studies were conducted using a ^{151}Sm:EuF_3 source. The measurements were done within a liquid nitrogen bath cryostat at 78 K. The source was kept under ambient conditions. The optimal sample thickness was calculated based on Long et al.,[37] and the ground sample was filled in a PMMA container (Ø = 20 mm) within a glovebox (argon atmosphere). The spectra were fitted using the WinNormos for Igor7 program package.[38] The final graphical editing was done with the program CorelDRAW2018.[39]

https://doi.org/10.1021/jacs.5c19173
J. Am. Chem. Soc. XXXX, XXX, XXX−XXX

Reflectance Spectroscopy

Diffuse reflectance spectra at room temperature were measured with an integrating sphere internally covered with BenFlect (reflectance R > 99% between 350 and 2000 nm) within an Edinburgh FLS1000 luminescence spectrometer. It was equipped with a 450 W Xe arc lamp, double Czerny-Turner excitation and emission grating monochromators and a thermoelectrically cooled (−20 °C) photomultiplier tube PMT-980 (Hamamatsu). Background was removed by measurements on a BenFlect-based blank. The spectra were corrected for the photomultiplier sensitivity, lamp intensity, and grating efficiency.

Investigations at High Pressures

A polycrystalline sample of $Eu_2Li(C_3)H$ was compressed and heated with a Hall-type six-ram large-volume press (mavo press LPQ6-1500-100; Max Voggenreiter GmbH, Germany) located at beamline P61B (DESY, Hamburg/Germany).[40] The experiments were performed using a standard 14/7 DESY assembly (Figure S5, Supporting Information) in 6−8 geometry with TF08 tungsten carbide cubes ($Fujilloy_{TM}$). A Cr_2O_3-doped MgO octahedron was used as a pressure-transmitting medium that contained a graphite sleeve for resistive heating. The sample pellet (Ø = 1 mm) was sealed in an airtight NaCl capsule (Ø = 3 mm), which was also used as a p/T-determinant using the in situ energy-dispersive X-ray diffraction (EDXRD) and the literature-known EoSs of NaCl.[41,42] During the experiment, the pressure was stepwise increased to 7.0(8) GPa, after which the sample was heated to approximately 1700(100) K in steps of ca. 50 K (estimated by the extrapolation of applied heating power/resulting temperature correlation data) while maintaining a pressure of 7 GPa. During the compression and throughout heating, the reaction was monitored by radiography and in situ EDXRD. Once the diffractogram became featureless, the temperature was lowered to room temperature, and the pressure was gradually decreased to ambient conditions. The PDIndexer software package,[43,44] TOPAS 5,[31] and EoSFit7[45] were used to analyze the EDXRD patterns. Pawley fits were performed on selected EDXRD measurements to obtain the lattice parameters of $Eu_2Li(C_3)H$ and NaCl using TOPAS 5.

Quantum Chemical Calculations (DFT)

Electronic structure calculations of RT- and LT-$Eu_2Li(C_3)H$ were carried out using density functional theory with Hubbard correction (DFT + U) and the generalized-gradient approximation for solids (PBEsol)[46] within the Quantum Espresso code.[47] Projector-augmented waves (PAW)[48−50] were used for the spin-polarized calculations. The energy cutoff was set to 1020 eV, and k-point grids of 7 × 7 × 13 (RT) and 5 × 5 × 13 (LT) were utilized for the two modifications. A Hubbard parameter of 3 eV was applied for the Eu 4f states, as suggested by the authors of the PAW pseudopotential,[49] to account for the strong local electron−electron interactions. Calculations of $Ca_2Li(C_3)H$[14] (energy cutoff: 1225 eV; k-point grid: 7 × 7 × 13), Mg_2C_3[34] (energy cutoff: 1225 eV; k-point grid: 9 × 11 × 15), $Eu_2Li(C_3)H$ (energy cutoff: 1020 eV; k-point grid: 7 × 7 × 13; vide supra), and H_2 (as molecule; unit cell: 30 × 30 × 30 Å^3; energy cutoff: 1020 eV; k-point grid: 4 × 4 × 4) were also performed as references and carefully checked for convergence. All compounds were structurally optimized with a convergence criterion of 10^{-3} eV for the ionic steps.

Chemical bonding analysis was conducted using the Local Orbital Basis Suite Toward Electronic Structure Reconstruction (LOBSTER).[51−55] This enabled the calculation of wave function-derived Löwdin charges,[56] Integrated Crystal Orbital Bond Indices (ICOBI),[57] and molecular-orbital analysis.[58] The basic sets included Eu (5s, 6s, 5p, 5d, 4f), Ca (3s, 4s, 3p, 4p), Mg (2s, 3s, 3p), Li (1s, 2s), C (2s, 2p), and H (1s). This resulted in low absolute charge spillings (<2.7%) in the calculations, as defined in LOBSTER. LOPOSTER[59] and Gnuplot[60] were used to evaluate and illustrate the data.

RESULTS AND DISCUSSION

Synthesis

By reacting lithium hydride and carbon black in a europium/lithium flux (molar ratio 10:7.7:5.5:2), single crystals of the novel compound $Eu_2Li(C_3)H$ were obtained. It crystallized in the form of black, shiny, and cuboid crystals (Figure S1, Supporting Information). The compound is highly sensitive to air and moisture and readily hydrolyzes under these conditions. The phase was thus treated and investigated under strict inert gas conditions.

The successful synthesis of $Eu_2Li(C_3)H$ demonstrates that a Eu/Li flux can be used as a metallic flux for the refractory element carbon, comparable to the use of a low-melting Ca/Li flux of the Latturner group for the preparation of new carbides and carbide hydrides.[14,17,18,61] It was also possible to replace lithium hydride by anthracene as a hydrogen source for a successful synthesis of $Eu_2Li(C_3)H$. In an attempt to substitute sodium for lithium in a Eu/Na flux with carbon black and anthracene (molar ratio 10:9.2:3.1:0.2), single crystals of EuC_2 (strongly twinned) and EuH_2 were obtained (Figure S6, Supporting Information). Using a high-resolution single-crystal X-ray diffraction measurement, the two hydrogen sites in EuH_2 could be localized in the difference Fourier map (1.20 e/Å^3 and 1.16 e/Å^3; Figure S7, Supporting Information) and were refined isotropically. Since previous structural solutions and refinements of EuH_2 (EuD_2) were, to the best of the authors' knowledge, conducted on powder samples only,[62−64] the crystallographic results have been added to Tables S1 and S2 (Supporting Information). The results are of relevance as neutron diffraction is difficult for europium hydrides due to the high absorption cross-section of the natural isotopic composition of europium combined with the large incoherent scattering of hydrogen.[65,66] The crystallographic data for EuH_2 derived from the single-crystal measurement in this work agree well with the results obtained by neutron diffraction of powdered EuD_2.[64]

Crystal Structures

At room temperature, $Eu_2Li(C_3)H$ crystallizes in the tetragonal space group $P4/mbm$ (no. 127, Z = 2) isotypic to the calcium compound $Ca_2Li(C_3)H$[14] (Figure 1). Selected crystallographic

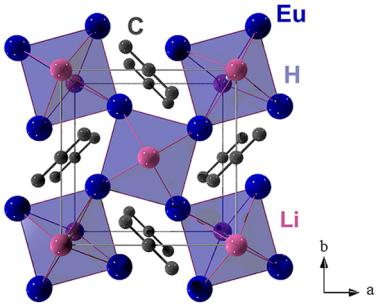

Figure 1. Crystal structure of RT-$Eu_2Li(C_3)H$; corner-linked Li_2Eu_4 tetragonal bipyramids are highlighted.

data are listed in Tables 1 and 2, with more detailed information in the Supporting Information (Tables S1 and S3). The structure can be described as a rotationally distorted antiperovskite type structure ABX_3 in which the anions' positions are occupied by allylenide (A) and hydride ions (B). Thus, the vertex-connected tetragonal bipyramids consisting of four equatorial europium and two axial lithium ions (X) are

https://doi.org/10.1021/jacs.5c19173
J. Am. Chem. Soc. XXXX, XXX, XXX−XXX

rotated against each other in the *ab* plane (Glazer notation $a^0a^0c^+$).[67] The centers of these distorted "octahedra" (δ = 12.474 using Polynator[68]) are occupied by hydride ions on Wyckoff site 2*b*. After the initial structure refinement without the assignment of the hydride ions, a residual electron density of 1.29 e/Å^3 was present in the distorted tetragonal bipyramidal voids (Figure S2, Supporting Information). Hydrogen could be successfully refined isotropically on this site. In accordance with the refinement for the compound $Ca_2Li(C_3)H$, the occupancy of the hydride site was set to 100%,[14] resulting in a charge-balanced description. The Eu···H distances within the tetragonal bipyramids are 2.6047(2) Å, which is significantly larger than the measured shortest contacts in EuH_2 (2.40(2) Å). In contrast, the Li···H distances (1.9668(2) Å) are shorter than those found in binary LiH (2.0417(3) Å).[35] The relatively short Li···H contacts along linear chains in the crystallographic *c* direction are consistent with the results for $Ca_2Li(C_3)H$, in which these Li···H distances are even shorter (1.8759(1) Å).[14]

The second anion in the compound is an allylenide ion C_3^{4-}, a rare species in carbide chemistry and first observed in Sc_3C_4[69] and $Ca_3Cl_2C_3$.[70] It resides in a distorted cuboctahedral void surrounded by eight europium and four lithium ions (Figure 2). The crystallographically distinct carbon atoms

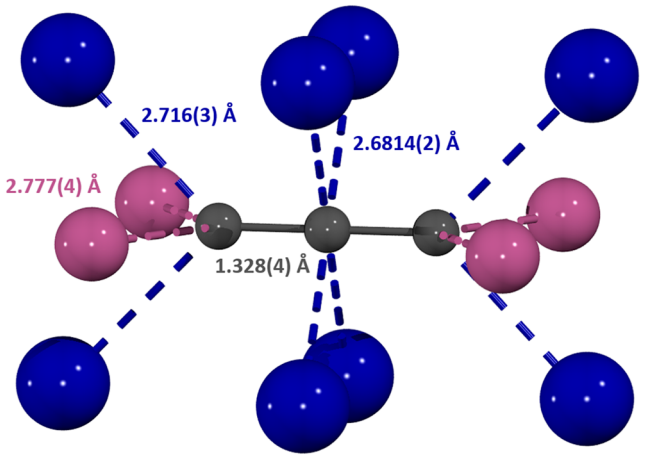

Figure 2. Coordination sphere around the allylenide anion in RT-$Eu_2Li(C_3)H$. Metal···carbon contacts are given as broken lines; color coding is as in Figure 1.

occupy the two Wyckoff sites 2*d* and 4*g*. The C−C bond length in the linear allylenide anion is 1.328(4) Å, which is in good agreement with a C−C double bond (1.34 Å).[71] In addition, the shortest Eu···C distances of 2.6814(2) Å (Eu···C1) and 2.716(3) Å (Eu···C2) are slightly shorter than those found in the acetylide compound EuC_2 (2.733(7) Å).[7] This may be interpreted as stronger metal−carbon bonds between these ions in $Eu_2Li(C_3)H$ (see the electronic structure calculations). Conversely, the Li···C contacts are significantly longer (2.777(4) Å) compared to those in binary lithium acetylide, Li_2C_2 (2.2122(6) Å and 2.4017(6) Å).[72]

The tetragonal unit cell of the europium compound (Table 1) is somewhat larger than that of the calcium congener (a = 6.8236(1) Å; c = 3.7518(1) Å).[14] This is in agreement with the larger ionic radii of Eu^{2+} (1.17 Å, CN = 6) compared to Ca^{2+} (1.00 Å; CN = 6)[73] and can be considered as a first indication for the presence of a divalent europium cation (r(Eu^{3+}) = 0.947 Å for CN = 6)[73] in $Eu_2Li(C_3)H$. Surprisingly, despite the similar ionic radii of Eu^{2+} and Sr^{2+} (1.18 Å; CN = 6),[73] we were unable to synthesize an analogous strontium compound $Sr_2Li(C_3)H$ to date. Instead, single crystals of SrC_2 and SrH_2 were obtained under similar synthesis conditions.

Perovskite-type compounds ABX_3 are well-known for their tendency to undergo phase transitions at different temperatures/pressures due to tilting and rotation of their $BX_{6/2}$ octahedra.[67] When a crystal of $Eu_2Li(C_3)H$ was cooled from room temperature to 240 K on a single-crystal X-ray diffractometer, the formation of superstructure reflections in the recorded precession images became apparent (Figure S8, Supporting Information). The structure of the resulting LT modification at 240 K could be solved and refined as a pseudo merohedral twin (twin law 010 100 00−1) from single-crystal XRD data (Tables 2, S1, and S4, Supporting Information). At 100 K, problems with data integration occurred and structure refinement due to a stronger orthorhombic distortion and twinning, which led to reflection splitting/broadening, became impossible. For this reason, Rietveld refinements of temperature-dependent high-resolution synchrotron powder diffraction data of $Eu_2Li(C_3)H$ (293 to 100 K) were conducted, and the result for the crystal structure obtained at 100 K (Tables 2 and S5−S7, Supporting Information) is discussed below alongside with the single-crystal data.

The LT modification of $Eu_2Li(C_3)H$ crystallizes in a new structure type in the orthorhombic space group *Pbam* (no. 55), a subgroup of *P*4/*mbm* (no. 127), with a doubled unit cell volume (Table 1; for details, see Figure S9, Supporting Information). The structural relationship between the RT and LT modifications is illustrated in Figure 3 using a reduced form of the *Bärnighausen* tree.[74] The full *Bärnighausen* tree is given in Figure S9 (Supporting Information), which was deduced with the help of ISODISTORT.[75,76] The largest structural distortion is found for the lithium ions, whose site symmetry is lowered and which move primarily along the orthorhombic *b*-axis with this new degree of freedom. This causes the ideal tetragonal bipyramid (δ = 0 (270 K)) around the hydride ion to become increasingly distorted during the phase transition (δ = 2.370 (240 K), δ = 5.688 (100 K)),[68] as the lithium ions in particular migrate from their ideal apical positions. The lithium ions exhibit a relatively high displacement within the *ab* plane already in the RT modification (Figure S10, Supporting Information), which can be regarded as a "harbinger" of the phase transition at lower temperatures. In addition, the LT modification now contains two crystallographically independent allylenide ions, which are slightly rotated (2.6(2)° and 1.7(1)°; 240 K) within the *ab* plane (Figure S11, middle, Supporting Information). As a result, the shortest Li···C distance of 2.777(4) Å in the RT modification is now split in shorter and longer distances for both independent allylenide ions in the LT modification (2.638(9) Å/2.923(9) Å and 2.655(10) Å/2.913(10) Å; 240 K). At lower temperatures (100 K), even shorter Li···C bonds are found (2.50(4) and 2.49(3) Å), even though these contacts are still significantly longer than those observed in Li_2C_2 (*vide supra*). These structural distortions can also be found in the Eu···Li and Eu···Eu contacts (Table S5, Supporting Information). From another perspective, the RT structure of $Eu_2Li(C_3)H$ is related to the U_3Si_2 structure type (or as ternary coloring variant the Mo_2B_2Fe structure type), which exhibits a variety of distortion variants in lower-symmetry superstructures.[77] These dislocations occur when the radii of the respective atoms do not fit precisely into the high-symmetry alignment, thereby often

https://doi.org/10.1021/jacs.5c19173
J. Am. Chem. Soc. XXXX, XXX, XXX−XXX

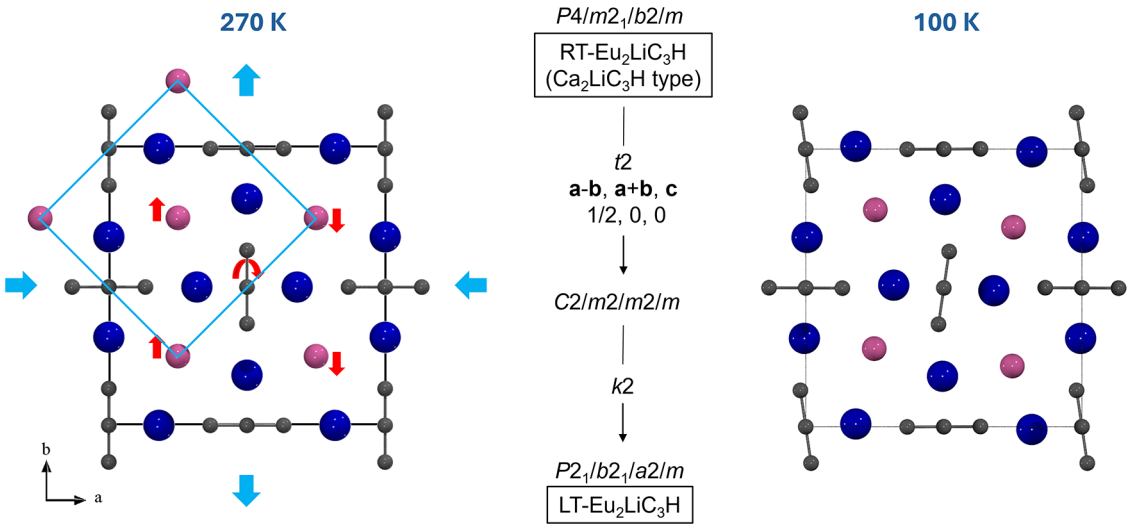

Figure 3. Center: reduced form of the *Bärnighausen* tree; views of the RT (left) and LT modifications (right) of $Eu_2Li(C_3)H$ in a view along [001]. Main structural distortions are indicated by arrows on the left; the primitive unit cell of the RT modification is outlined in turquoise.

enabling a strengthening of (metallic) bonds.[78] A further bonding analysis for both modifications will be carried out later (see the electronic calculations). As an analogous phase transition has not been reported for $Ca_2Li(C_3)H$ down to 150 K,[14] it is assumed that the larger Eu^{2+} ions in $Eu_2Li(C_3)H$ expand the coordination sphere for the anions in such a way that structural distortions occur at low temperatures in order to better accommodate these anions (puckering effect).[79]

Beside the single-crystal structure analysis, the phase transition of $Eu_2Li(C_3)H$ was monitored by *in situ* X-ray powder diffraction using synchrotron radiation (BL9, DELTA, Dortmund/Germany) upon cooling from 293 to 100 K (Figure S12, Supporting Information). In the measured powder diffraction patterns, both the evolution of superstructure reflections (Figure S13, Supporting Information) and the splitting of several reflections during the phase transition to the orthorhombic modification is observed (Figure 4, top). Rietveld refinements were used to determine the development of the lattice parameters (Figure 4, bottom) and the progression of structural distortions with the temperature. It is apparent from the progression of the lattice parameters that the phase transformation starts during cooling at approximately 250 K and splits the tetragonal *a* axis into the two orthorhombic *a* and *b* axes, while the *c* axis shows the expected temperature-induced shortening. The structural models for the LT modification obtained from Rietveld refinements also exhibit the discussed progression of structural distortions at low temperatures and are thus consistent with the results from the single-crystal data (Figure S11 in the Supporting Information).

The temperature-induced phase transition can be classified as displacive,[80] due to the relatively small atomic movements/shifts during the structural changes. Furthermore, the continuous splitting of the *a* and *b* axes (Figure 4, bottom), the steady volume change (Figure S14, Supporting Information), and the unobserved coexistence of the two phases indicate a second-order phase transition.[81] In full agreement with this, a group−subgroup relationship can be developed for the transition from the RT to the LT modification (Figures 3 and S9, Supporting Information). Warming $Eu_2Li(C_3)H$ to room temperature after cooling leads to a reversible transformation back to the RT modification.

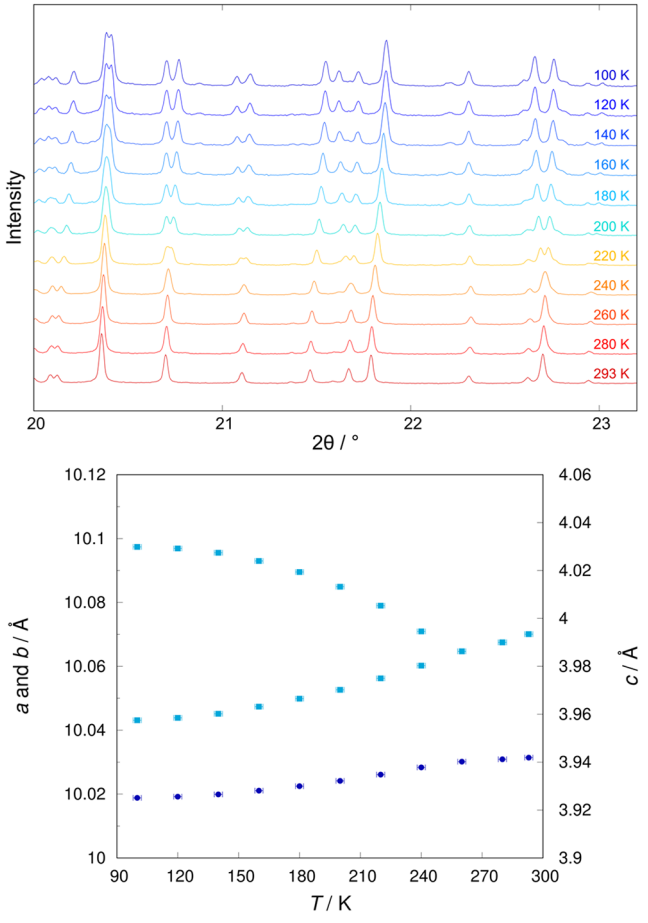

Figure 4. Top: sections of synchrotron powder diffraction patterns of $Eu_2Li(C_3)H$ upon cooling (from 293 K (bottom) to 100 K (top)) with symmetry-induced splitting of some reflections during phase transition; bottom: temperature-dependent progression of the lattice parameters of $Eu_2Li(C_3)H$ upon cooling (*c*: dark blue; *a*,*b*: light blue); note: above the phase transition temperature, a_{tet} is multiplied by $\sqrt{2}$ for a clearer presentation.

https://doi.org/10.1021/jacs.5c19173
J. Am. Chem. Soc. XXXX, XXX, XXX−XXX

IR and GC Measurements

To further confirm the existence of an allylenide ion within the structure of $Eu_2Li(C_3)H$, IR and GC measurements were carried out. In the IR spectrum (Figure 5, top), the vibration at

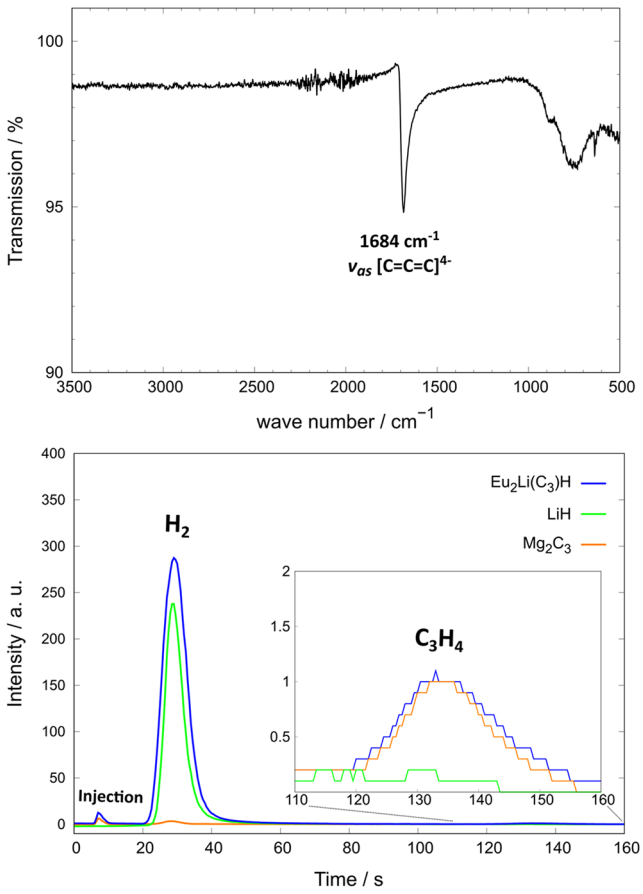

Figure 5. Top: IR spectrum of $Eu_2Li(C_3)H$; bottom: GC spectra of gaseous products of $Eu_2Li(C_3)H$ after hydrolysis with water. LiH (H_2) and Mg_2C_3 (C_3H_4) were used as references. The injection peak is an artifact of the instrument and can be neglected.

1684 cm^{-1} can be assigned to the IR active antisymmetric stretching mode ν_{as} of the allylenide ion. This value is close to the measured IR signal ν_{as} = 1668 cm^{-1} for the allylenide ion in $Ca_3Cl_2C_3$.[70] An additional sharp signal appears at 638 cm^{-1} and is within the range of the reported values for the bending mode δ of C_3 units in $Ba_{12}InC_{18}H_4$ (593 cm^{-1})[18] and $Ca_{11}Sn_3C_8$ (589 cm^{-1}).[17] The symmetric stretching mode of the linear C_3^{4-} anion is typically IR inactive but Raman active. However, due to the metallic/reflective nature of $Eu_2Li(C_3)H$, recording of a Raman spectrum was not successful.

Since the hydrolysis products of ionic carbides are characteristic for their anions,[2] the gaseous hydrolysis products of $Eu_2Li(C_3)H$ were analyzed using a home-built gas chromatograph (see Experimental Section). For allylenide compounds, the formation of the isomers allene (propadiene) and/or propyne (both C_3H_4), as observed during the hydrolysis of Mg_2C_3,[82] is to be expected. By comparison with reference substances (LiH and Mg_2C_3), the formation of hydrogen (H_2) and propyne/allene (C_3H_4) as gaseous hydrolysis products of $Eu_2Li(C_3)H$ is evident (Figure 5, bottom), which further confirms the presence of an allylenide ion. Note: our method does not allow to distinguish between allene and propyne. The presence of a hydride ion cannot be verified beyond any doubt in these measurements, as in some cases, small flux residues were present on the crystals (Eu < 2 wt % according to PXRD data; Figure S3, Supporting Information). However, the large signal in Figure 5 (bottom) suggests that hydrogen (H_2) is not formed from small amounts of an impurity, but hydrolysis could lead to the oxidation of Eu(II) to Eu(III) and thus to the formation of hydrogen. Furthermore, no other molecule indicative of a third anion in $Eu_2Li(C_3)H$ was detected.

Thus, the title compound $Eu_2Li(C_3)H$ is the first europium carbide with an allylenide anion, since the few known compounds contain either C_2 units, namely, EuC_2[7] and $Eu_{3.16}NiC_6$,[12] or isolated carbon atoms ($EuRh_3C$).[83] Considering the results for $Ca_2Li(C_3)H$ and the formulation of a charge-balanced composition (see below), it is most likely that hydride sites 2*b* are fully occupied. This would be in contrast to other lanthanide carbide hydrides ($LaCH_x$, Yb_2CH_x),[84] in which interstitial hydrogen atoms are present in tetrahedral sites with partial occupancies. To fully verify the occupancy of the hydride site in $Eu_2Li(C_3)H$, a neutron diffraction experiment using a deuteride might be attempted in future, analogous to the measurements on EuD_2 and $EuLiD_3$.[64] However, due to the high absorption cross-section of europium mentioned above, this is not a simple task and requires a flat-plate technique.

Magnetic Properties

Figure 6 (inset) displays the temperature dependence of the inverse magnetic susceptibilities of $Eu_2Li(C_3)H$, measured at a

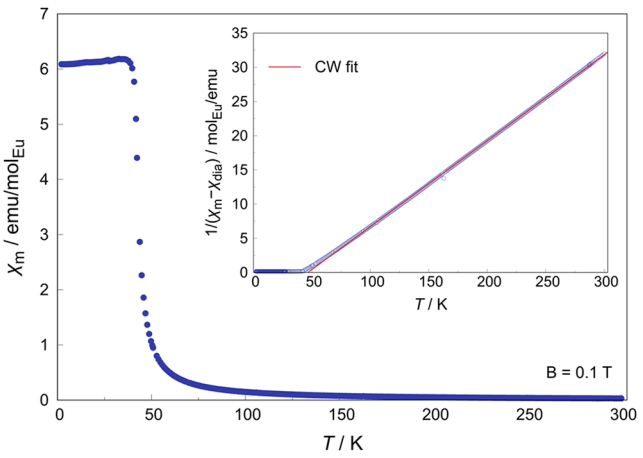

Figure 6. Temperature dependence of magnetic susceptibilities and inverse magnetic susceptibilities (inset) of $Eu_2Li(C_3)H$ measured at B = 0.1 T. The red line shows the Curie–Weiss fit (see text).

magnetic flux density of 0.1 T. Above 70 K, Curie–Weiss behavior is visible in the $1/(\chi_m-\chi_{dia}) = f(T)$ plot. From a Curie–Weiss fit, according to

$$1/(\chi_m - \chi_{dia}) = (T - \theta)/C$$

an effective magnetic moment μ_{eff} = 7.98(1) μ_B/Eu and a Weiss constant θ = 46.5(1) K are obtained. The resulting effective magnetic moment is close to the expected value for a free Eu^{2+} ion (7.94 μ_B, spin only value). The measured saturation moment μ_{sat} = 6.56 μ_B (Figure S15, Supporting Information) is also in the range of the expected value for Eu^{2+} (μ_{sat} = 7 μ_B).

https://doi.org/10.1021/jacs.5c19173
J. Am. Chem. Soc. XXXX, XXX, XXX−XXX

The results of the magnetochemical investigations clearly indicate the existence of divalent europium in $Eu_2Li(C_3)H$. This low oxidation state is probably a consequence of the only modest oxidizing power of carbon and hydrogen. Together with the results of the GC and structural investigations, a charge-balanced ionic limit formula $(Eu^{2+})_2Li^+(C_3)^{4-}H^-$ can be deduced. The obtained positive Weiss constant θ is indicative of ferromagnetic interactions in the paramagnetic regime. A transition to a ferromagnetic state is indeed observed below the Curie temperature T_C = 42 K (Figure 6), which was precisely determined using the derivative $d\chi_m/dT$ (Figure S16, Supporting Information). Compared to the ferromagnetic binary compounds EuC_2 (T_C = 15 K)[7] and EuH_2 (T_C = 18 K),[85] the Curie temperature of $Eu_2Li(C_3)H$ is rather high. There is no indication of ferromagnetic contamination of the measured sample by EuO (T_C = 69 K). Furthermore, no feature related to the structural phase transition was found in the temperature-dependent magnetic susceptibility data. The measured magnetization curve $M(B)$ for $Eu_2Li(C_3)H$ shows a very small hysteresis (Figure S17, Supporting Information), which classifies the compound as a soft ferromagnetic material. EuC_2 exhibits a similar behavior,[7] which is a typical feature for compounds with divalent europium.[86]

^{151}Eu Mössbauer Spectroscopy

The ^{151}Eu Mössbauer spectra of $Eu_2Li(C_3)H$ at room temperature (top) and 78 K (bottom) are presented in Figure 7. The corresponding fitting parameters are listed in Table 3.

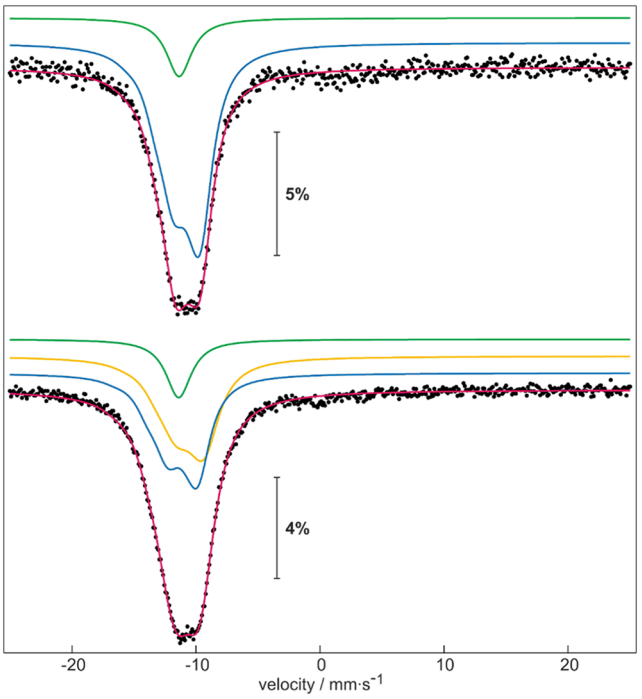

Figure 7. Experimental (dots) and simulated (colored lines) ^{151}Eu Mössbauer spectra of $Eu_2Li(C_3)H$ at room temperature (top) and 78 K (bottom).

The room-temperature spectrum (Figure 7, top) was fitted with the superposition of two signals. The main signal (85(1) %) shows an isomer shift of δ = −10.9(2) mm s^{-1} and exhibits a quadrupole splitting of ΔE_Q = 5.8(2) mm s^{-1}. This isomer shift is in the range prominent for divalent europium, and the quadrupole splitting is consistent with the noncubic site symmetry of the 4*h* europium site (*m*.2*m*) in the space group *P*4/*mbm* (no. 127). The line width of Γ = 2.35(6) mm s^{-1} is in the usual range for ^{151}Eu Mössbauer-spectroscopic measurements. There are not many ^{151}Eu Mössbauer spectra known for compounds with a similar composition. Two examples are the carbide EuC_2 (δ = −11.78(3) mm s^{-1})[7] and the hydride $EuLiH_3$ (δ = −11.8(2) mm s^{-1}).[87] Comparison of these results with $Eu_2Li(C_3)H$ shows a less negative isomer shift for the title compound, indicating a lower *s*-electron density.

Table 3. Fitting Parameters of ^{151}Eu Mössbauer Spectroscopic Measurements for $Eu_2Li(C_3)H$ at Room Temperature and 78 K[a]

signal	δ/mm s^{-1}	ΔE_Q/mm s^{-1}	Γ/mm s^{-1}	ratio/%
		Room Temperature		
blue	−10.9(2)	5.8(2)	2.35(6)	85(1)
green	−11.36(8)	0*	2.5*	15
		78 K		
blue	−11.29(5)	6.5(2)	2.4(2)	43(1)
yellow	−10.66(7)	6.2(4)	2.9(2)	43
green	−11.40(8)	0*	2.5*	14

[a]δ = isomer shift, ΔE_Q = quadrupole splitting parameter, and Γ = experimental line width. Parameters marked with an asterisk were kept fixed during the fitting procedure.

The second signal (15%) with an isomer shift of δ = −11.36(8) mm s^{-1} is probably caused by a decomposition product, since $Eu_2Li(C_3)H$ is highly sensitive to hydrolysis. This signal could be assigned to EuO (δ = −11.28(11) mm s^{-1}),[88] which is confirmed by the results of X-ray powder diffraction data. The quadrupole splitting of this subspectrum was kept fixed at ΔE_Q = 0 mm s^{-1}, as the europium site shows a cubic site symmetry (4*a*) in rocksalt-type EuO[89] and the low intensity of the subsignal in combination with the overlap of the signals in the spectrum do not allow for a separate refinement due to excessive correlation. For the same reasons, the line width was kept fixed at Γ = 2.5 mm s^{-1}.

The spectrum at 78 K (Figure 7, bottom) could be fitted with a superposition of three signals, two main signals with equal areas (43(1)%:43%) and a third signal (14%). The structure shows a phase transition at ca. 250 K, which results in a splitting of the 4*h* europium subcell site in the high-temperature phase (space group *P*4/*mbm*, no. 127) to two 4*h* sites in the low-temperature structure (space group *Pbam*, no. 55); see discussion of the crystal structures. The signal ratios of the two main signals were kept identical (1:1 (blue and yellow)) in the final refinement to account for the two independent Eu sites with the same multiplicity.

The two signals of equal intensity can be assigned to the two 4*h* sites with the isomer shifts of δ = −11.29(5) mm s^{-1} (blue) and δ = −10.66(7) mm s^{-1} (yellow). The signals show quadrupole splittings of ΔE_Q = 6.5(2) mm s^{-1} and ΔE_Q = 6.2(4) mm s^{-1}, respectively. Both europium sites have a coordination number of 10 and are coordinated by hydride and allylenide anions. They slightly differ with respect to the interatomic distances (see Table S5, Supporting Information), which explains the different isomer shifts. However, an assignment based on the DFT calculations given below was not possible, as very similar occupancies of 6*s* orbitals were obtained for both sites. The third subsignal corresponds to EuO,[88] as discussed for the room-temperature phase. Unfortunately, no measurements below the Curie

https://doi.org/10.1021/jacs.5c19173
J. Am. Chem. Soc. XXXX, XXX, XXX−XXX

temperature were possible, because no suitable cryostat was available.

High-Pressure, High-Temperature (HPHT) Investigations

Due to the smaller ionic radius of Eu^{3+} (r = 0.947 Å, CN = 6) compared to Eu^{2+} (1.17 Å, CN = 6),[73] valence changes from Eu^{2+} to Eu^{3+} have been observed upon the application of pressure for EuO[90] and many other europium compounds.[91] To verify such a behavior for $Eu_2Li(C_3)H$, we conducted HPHT investigations at beamline P61B (DESY, Hamburg/Germany).[40] To our surprise, no such behavior was observed even up to 7 GPa, as apparent from a heatmap resulting from progressively recorded in situ EDXRD patterns under HPHT conditions (Figure 8). $Eu_2Li(C_3)H$ shows a continuous

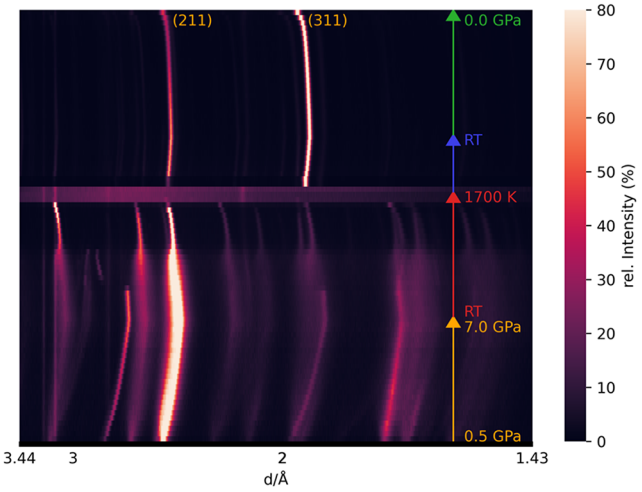

Figure 8. Heatmap of in situ EDXRD measurements (beamline P61B, DESY, Hamburg/Germany). The progression of reaction conditions is indicated by arrows on the right-hand side of the heatmap (bottom to top): compression, heating, cooling, decompression.

decrease of the unit cell volume upon compression, which can be described by applying a third-order Birch-Murnaghan equation of the state model (BM3 EoS) in EoSFit7[45] (Figure S18, Supporting Information). This results in a bulk modulus of K_0 = 65 GPa with V_0 = 199.88(5) Å^3, K' = 1.8, and K'' = −0.0992 GPa^{-1} (fixed). With increasing temperature during the heating phase of the experiment at ∼7 GPa, the unit cell volume expands, which was fitted with the *Berman* thermal model[92] using EoSFit7[45] (Figure S19, Supporting Information) to calculate the volumetric thermal expansion coefficients: $\alpha_0 = 9.9 \times 10^{-5}$ K^{-1} and $\alpha_1 = -15.6 \times 10^{-5}$ K^{-2} at T_{ref} = 300 K. The former value is similar to that obtained for europium metal at 293 K: $\alpha = 12.3 \times 10^{-5}$ K^{-1}.[93] At approximately 1700 K, the sample finally melted (see photos, Table S8, Supporting Information) and was then cooled and decompressed. The EDXRD patterns mainly show two prominent reflections, (211) and (311), which can be attributed to the recrystallized sample in a single-crystalline and oriented form. *Ex situ* SCXRD measurements confirmed the known unit cell of RT-$Eu_2Li(C_3)H$. Its high stability under drastic HPHT conditions (7 GPa, 1700 K) is remarkable.

Electronic Structure Calculations

The title compound contains a linear C_3^{4-} anion with $D_{\infty h}$ symmetry, which is isoelectronic to CO_2. Figure 9 (left) depicts the MO diagram for the C_3 unit in RT-$Eu_2Li(C_3)H$, reconstructed from a spin-polarized DFT+U calculation (U_f = 3 eV) using LOBSTER.[54] In addition, the molecular orbitals near the Fermi level, E_F, including HOMO and LUMO, are illustrated. The 16-electron anion is formally populated up to the π_g molecular orbitals ($1e_{1g}/2e_{1g}$) as a HOMO.

The contributions and energetic order of the individual molecular orbitals are also evident in the calculated density of states (DOS) of $Eu_2Li(C_3)H$ (Figure 9, middle), where interactions with neighboring atoms lead to broadening. Besides the occupied states of the C_3^{4-} anion and the hydride ion just around −4 eV, the valence bands are mainly dominated by the localized 4*f* states of europium near the Fermi level. In accordance with the experimental data, a ferromagnetic ground state was calculated. In contrast, the conduction bands are mainly formed by the 5*d* states of europium.

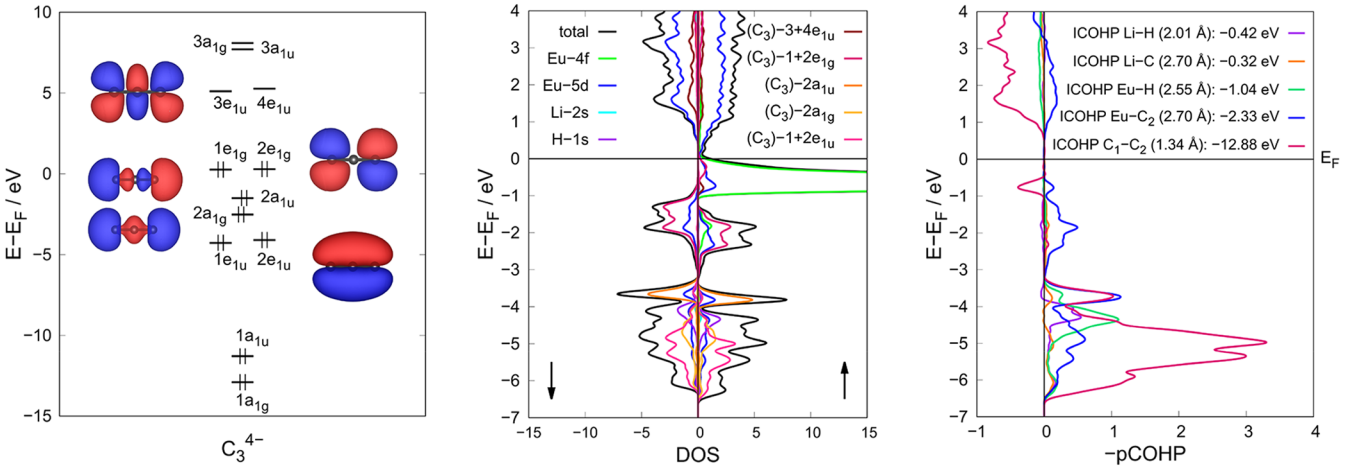

Figure 9. Left: molecular-orbital diagram of the C_3^{4-} unit in $Eu_2Li(C_3)H$. Both spin channels were averaged for each MO. Images for MOs near the Fermi level are plotted (note: only one of the two π orbitals is shown). Middle: AO- and MO-resolved DOS data showing the contributions of selected atomic and molecular orbitals near the Fermi level (black arrows indicate the two spin channels). Right: projected crystal orbital Hamilton population (pCOHP) bonding analysis for selected contacts in $Eu_2Li(C_3)H$. Integrated COHP (ICOHP) values are listed in the upper right corner together with the optimized distances.

https://doi.org/10.1021/jacs.5c19173
J. Am. Chem. Soc. XXXX, XXX, XXX−XXX

Furthermore, the DOS shows a pseudogap near the Fermi level, which would characterize the compound as a poor metal, and is in agreement with the charge-balanced ionic description given above. Calculated Löwdin charges and Madelung energy (Table S9, Supporting Information) also reveal a substantial ionic bonding contribution, allowing the compound to be classified as a Zintl phase. This is in line with the results from the ^{151}Eu Mössbauer-spectroscopic measurements, whose isomer shift of $\delta = -10.9(2)$ mm s^{-1} (Figure 7) is within the range of other europium-containing Zintl phases (e.g., EuZnSn, $\delta = -10.76$ mm s^{-1}).[94] Compared to other allylenide compounds, such as Mg_2C_3 (E_g = 1.6 eV) and (at RT) isotypic $Ca_2Li(C_3)H$ (E_g = 1.2 eV), the transition from ionic to more covalent/metallic behavior by the incorporation of europium ions is evident from the calculated band gaps and Löwdin charges (Table S9, Supporting Information). Due to the high air sensitivity of the compound, it was not possible to date to measure the temperature-dependent electrical conductivity to confirm the calculated metallic behavior. However, a diffuse reflectance measurement (Figure S20, Supporting Information) shows almost complete reflectivity all over the visible range without detectable absorption edges, which additionally supports metallic behavior of $Eu_2Li(C_3)H$. This is consistent with the black, shiny appearance of the crystals. Even upon the application of significantly higher Hubbard localization energies U_f (8 eV) in the calculations, the compound was predicted to be metallic according to these calculations.

When the strength of the interactions within $Eu_2Li(C_3)H$ is examined using a pCOHP analysis, it is noticeable that the strongest individual bond is within the $[C{=}C{=}C]^{4-}$ anion (Figure 9 (right) and Figure S21, Supporting Information). A bond order (ICOBI) of 1.57 is calculated for the formal C=C double bond. This value is lower than the one calculated for the allylenide ion in Mg_2C_3 (1.80), which is probably a consequence of the stronger nonionic interactions of the C_3 unit in $Eu_2Li(C_3)H$ with its coordination environment and the increased metallicity. The strongest individual interaction between the allylenide ion and its environment arises from the terminal carbon atoms and the "end-on"-coordinated europium ions (Figure 2). The interactions from the "side-on"-coordinating europium ion with the terminal C atom (−0.96 eV/bond) and the central C atom (−1.13 eV/bond) are individually weaker, but notably, the former bond occurs twice. In comparison, the Eu−H, Li−H, and Li−C interactions are significantly weaker (Figure 9 (right), and Figure S21, Supporting Information), although substantial Eu−Eu interactions are found. The bonding within the C_3^{4-} unit was analyzed in more detail using a MOFE (molecular-orbital formation energy) diagram, which is discussed in the Supporting Information (Figure S22).

For the LT modification, the ICOHP analysis reveals a splitting of the bond strengths in the case of the Eu−Li and Li−C interactions at low temperatures (Figure S21, Supporting Information). This is consistent with the observed structural distortion and the resulting differing bond distances. However, when considering the average bonding strength (i.e., the mean ICOHP), there is little change in the calculated bond strengths for the Eu−Li (from −0.423 eV/bond for RT-$Eu_2Li(C_3)H$ to −0.434 eV/bond for LT-$Eu_2Li(C_3)H$) and Li−C contacts (from −0.315 to −0.314 eV/bond) during the phase transition. With regard to ionic bonding contributions, only a small increase in Madelung energy was calculated for the LT modification (from −370 to −389 kJ/mol), resulting from minor increases in the Löwdin charges of the europium ions and the terminal C atom of the C_3 moiety. To analyze and rationalize the electronic structure and phase transition of $Eu_2Li(C_3)H$ in more detail, temperature-dependent resistivity measurements should be addressed in future investigations, but due to the very high sensitivity of the title compound to air and moisture, they will pose a major challenge.

Further confirmation for the presence of a hydride anion in the title compound was gained from analysis of the total energies (for the RT modification) according to the following reaction equation:

$$Eu_2Li(C_3) + 1/2H_2 \rightarrow Eu_2Li(C_3)H$$

For $Mg_5Bi_3H_x$, this method recently supported the proposed hydrogen incorporation.[95] $Eu_2Li(C_3)H$ was calculated to be −125.4 kJ/mol more stable than the left part of the equation, which further supports the presence of a hydride anion.

CONCLUSIONS

Using a Eu/Li flux as a solvent, we were able to synthesize single crystals of the new compound $Eu_2Li(C_3)H$. This reveals a europium−lithium mixture as an attractive reaction medium for the synthesis of novel europium carbides and hydrides, for which only a few examples exist in the literature, despite their potentially attractive properties. At room temperature, $Eu_2Li(C_3)H$ crystallizes in the tetragonal space group $P4/mbm$ (no. 127, Z = 2) analogous to $Ca_2Li(C_3)H$.[14] Below ∼250 K, a phase transition to an orthorhombic modification ($Pbam$, no. 55, Z = 4) was observed. The transition follows a group−subgroup relationship and is accordingly classified as a second-order phase transition. The existence of a first europium compound with an allylenide ion (C_3^{4-}) was further confirmed by IR and GC investigations. Measurements of the magnetic susceptibilities and ^{151}Eu Mössbauer spectra verified a divalent state of the europium ion in $Eu_2Li(C_3)H$, resulting in a charge-balanced description: $(Eu^{2+})_2(Li^+)(C_3^{4-})(H^-)$. A transition to a ferromagnetic ground state at a Curie temperature of T_C = 42 K was observed. This T_C is remarkably high compared to the binary compounds EuC_2 (T_C = 15 K)[7] and EuH_2 (T_C = 18 K).[85] It is conceivable that the peculiar electronic properties of $Eu_2Li(C_3)H$ with an almost negligible band gap are responsible for this. However, more detailed experimental and theoretical analyses are needed to confirm this assumption. Based on the current findings and electronic structure calculations, the title compound can be classified as a Zintl phase, whose bonding is a combination of ionic and covalent/metallic contributions and very much dominated by the molecular C_3^{4-} anion.

When replacing the Eu/Li by a Eu/Na flux, single crystals of EuH_2 (and EuC_2) were obtained with carbon black and anthracene (molar ratio: 10:9.2:3.1:0.2) using a slightly different heating program. However, no analogous Eu−Na carbide hydride could be synthesized to date.

ASSOCIATED CONTENT

Supporting Information

The Supporting Information is available free of charge at https://pubs.acs.org/doi/10.1021/jacs.5c19173.

Additional figures, photographs, schemes, data plots and tables (PDF)

https://doi.org/10.1021/jacs.5c19173
J. Am. Chem. Soc. XXXX, XXX, XXX−XXX

Accession Codes

Deposition numbers 2488130−2488132 and 2488135 contain the supporting crystallographic data for this paper. These data can be obtained free of charge via the joint Cambridge Crystallographic Data Centre (CCDC) and Fachinformationszentrum Karlsruhe Access Structures service.

AUTHOR INFORMATION

Corresponding Author

Uwe Ruschewitz − *Institute of Inorganic and Materials Chemistry, University of Cologne, D-50939 Cologne, Germany;* orcid.org/0000-0002-6511-6894; Email: uwe.ruschewitz@uni-koeln.de

Authors

Tim Kleinöder − *Institute of Inorganic and Materials Chemistry, University of Cologne, D-50939 Cologne, Germany;* orcid.org/0009-0004-7757-9978

Carolin Hoverath − *Institute of Inorganic and Materials Chemistry, University of Cologne, D-50939 Cologne, Germany;* orcid.org/0009-0005-7835-1075

Thomas Lorenz − *Institute of Physics II, University of Cologne, D-50937 Cologne, Germany;* orcid.org/0000-0003-4832-5157

Joshua Wiethölter − *Institut für Anorganische und Analytische Chemie, Universität Münster, D-48149 Münster, Germany;* orcid.org/0009-0006-8470-2764

Theresa Block − *Institut für Anorganische und Analytische Chemie, Universität Münster, D-48149 Münster, Germany*

Rainer Pöttgen − *Institut für Anorganische und Analytische Chemie, Universität Münster, D-48149 Münster, Germany*

Tom Förster − *Inorganic Photoactive Materials, Institute of Inorganic Chemistry, Heinrich Heine University Düsseldorf, 40225 Düsseldorf, Germany*

Markus Suta − *Inorganic Photoactive Materials, Institute of Inorganic Chemistry, Heinrich Heine University Düsseldorf, 40225 Düsseldorf, Germany;* orcid.org/0000-0001-8024-6665

Complete contact information is available at: https://pubs.acs.org/10.1021/jacs.5c19173

Author Contributions

The manuscript was written through contributions of all authors. All authors have given approval to the final version of the manuscript.

Notes

The authors declare no competing financial interest.

ACKNOWLEDGMENTS

Funding by the Deutsche Forschungsgemeinschaft DFG (project no. RU 546/15-1) is gratefully acknowledged by U.R., T.K., and C.H. M.S. gratefully acknowledges funding by the "Young College" of the North-Rhine Westphalian Academy of Sciences, Humanities, and the Arts. The authors thank Tim Mattick (for the help with measurements and data visualization) and Dr. Christian Sternemann as well as Dr. Michael Paulus (synchrotron powder data) for their help and support with data acquisition and DELTA for providing synchrotron radiation. We acknowledge DESY (Hamburg, Germany), a member of the Helmholtz Association HGF, for the provision of experimental facilities. Parts of this research were carried out at beamline P61B (Proposal No. I-20240299). The beamline LVP instrument Aster-15 is funded by the ErUM-Pro program (grants no.: 05K16WC2 and 05K13WC2) of the German Federal Ministry of Education and Research (BMBF), which also supported the research by the provision of a glovebox (grant no. 05K20OLA). In addition, we would like to thank Dr. Kristina Spektor and Dr. Shrikant Bhat for assistance with assembly preparation and beamline operation. We furthermore thank the ITCC (IT Center University of Cologne) for providing compute resources on the DFG-funded HPC (High Performance Computing) system RAMSES (Research Accelerator for Modeling and Simulation with Enhanced Security) as well as for their support (DFG funding number: INST 216/512-1 FUGG).

REFERENCES

(1) Pauling, L. The Nature of the Chemical Bond. IV. The Energy of Single Bonds and the Relative Electronegativity. *J. Am. Chem. Soc.* **1932**, *54* (9), 3570−3582.

(2) Ruschewitz, U. Binary and Ternary Carbides of Alkali and Alkaline-Earth Metals. *Coord. Chem. Rev.* **2003**, *244* (1−2), 115−136.

(3) Zhang, W. Recent Progress in B_4C−SiC Composite Ceramics: Processing, Microstructure, and Mechanical Properties. *Mater. Adv.* **2023**, *4* (15), 3140−3191.

(4) Nassaralla, C. L. Iron Production. In *Encyclopedia of Materials: Science and Technology*; Elsevier, 2001; pp 4296−4301.

(5) Zhang, J.; Hassan Saeed, M.; Li, S. Recent Progress in Development of High-Performance Tungsten Carbide-Based Composites. In *Advances in Ceramic Matrix Composites*; Elsevier, 2018; pp 307−329.

(6) Mori, T. Lanthanides: Boride, Carbide, and Nitride Compounds. In *Encyclopedia of Inorganic and Bioinorganic Chemistry*; Wiley, 2012.

(7) Wandner, D.; Link, P.; Heyer, O.; Mydosh, J.; Ahmida, M. A.; Abd-Elmeguid, M. et al. Structural Phase Transitions in EuC_2 *Inorg. Chem.* **2010**, *49* (1), 312-318.

(8) Atoji, M. Neutron Diffraction Studies of CaC_2, YC_2, LaC_2, CeC_2, TbC_2, YbC_2, LuC_2, and UC_2. *J. Chem. Phys.* **1961**, *35* (6), 1950−1960.

(9) Sales, B. C.; Wohlleben, D. K. Susceptibility of Interconfiguration-Fluctuation Compounds. *Phys. Rev. Lett.* **1975**, *35* (18), 1950−1960.

(10) Link, P.; Glatzel, P.; Kvashnina, K.; Smith, R. I.; Ruschewitz, U. Yb Valence States in YbC_2: A HERFD-XANES Spectroscopic Investigation. *Inorg. Chem.* **2011**, *50* (12), 5587−5595.

(11) Rida, H.; Cahen, S.; Hérold, C.; Lagrange, P. Bulk Synthesis and Crystal Structure of the First Stage Europium−Graphite Intercalation Compound. *Carbon* **2010**, *48* (11), 3190−3195.

(12) Witte, A. M.; Jeitschko, W. Preparation and Crystal Structure of the Isotypic Carbides $Ln_{3.67}TC_6$ (Ln = Rare Earth Elements; T = Mn, Fe, Ru) and $Eu_{3.16}NiC_6$. *Z. Naturforsch., B* **1996**, *51* (2), 249−256.

(13) Holleck, H. The Effect of Carbon on the Occurrence of Cu_3Au-Type Phases in Actinide-and Lanthanide-Platinum Metal Systems. *J. Nucl. Mater.* **1972**, *42* (3), 278−284.

(14) Lang, D. A.; Zaikina, J. V.; Lovingood, D. D.; Gedris, T. E.; Latturner, S. E. Ca_2LiC_3H: A New Complex Carbide Hydride Phase Grown in Metal Flux. *J. Am. Chem. Soc.* **2010**, *132* (49), 17523−17530.

(15) Jesche, A.; Canfield, P. C. Single Crystal Growth from Light, Volatile and Reactive Materials Using Lithium and Calcium Flux. *Philos. Mag.* **2014**, *94* (21), 2372−2402.

(16) Zaikina, J. V.; Zhou, H.; Latturner, S. E. Structural Relationships between New Carbide $La_{14}Sn(MnC_6)_3$ and Fully Ordered $La_{11}(MnC_6)_3$. *J. Solid State Chem.* **2010**, *183* (12), 2987−2994.

(17) Blankenship, T. V.; Lita, A.; Latturner, S. E. $Ca_{11}E_3C_8$ (E = Sn, Pb): New Complex Carbide Zintl Phases Grown from Ca/Li Flux. *Inorg. Chem.* **2012**, *51* (24), 13345−13350.

(18) Blankenship, T. V.; Dickman, M. J.; van de Burgt, L. J.; Latturner, S. E. $Ca_{12}InC_{13-x}$ and $Ba_{12}InC_{18}H_4$: Alkaline-Earth Indium Allenylides Synthesized in AE/Li Flux (AE = Ca, Ba). *Inorg. Chem.* **2015**, *54* (3), 914−921.
(19) Engstrand, T. O.; Cope, E. M.; Vasquez, G.; Haddock, J. W.; Hertz, M. B.; Wang, X.; Latturner, S. E. Flux Synthesis of a Metal Carbide Hydride Using Anthracene As a Reactant. *Inorg. Chem.* **2020**, *59* (16), 11651−11657.
(20) Larson, J. T.; Wix, K. D.; Chen, B.; Latturner, S. E. Metal Flux Growth of Lanthanide Carbide Hydrides Using Anthracene. *Inorg. Chem.* **2023**, *62* (33), 13277−13283.
(21) Marzano, L.; Uddin, M. S.; Zareihassangheshlaghi, A.; Araoyinbo, O.; Hernandez, J.; Latturner, S. Flux Growth of La_3MC_2 (*M* = Sb, Bi, Te), a New Family of Ternary Carbides. *Z. Anorg. Allg. Chem.* **2025**, *651*, No. e202500046.
(22) Ma, X.; Lu, J.; Whalen, J. B.; Latturner, S. E. Flux Growth and Magnetoresistance Behavior of Rare Earth Zintl Phase EuMgSn. *Inorg. Chem.* **2013**, *52* (6), 3342−3348.
(23) Bruker AXS Inc. *SAINT* Madison, Wisconsin, USA, 2012.
(24) Bruker AXS Inc. *SADABS* Madison, Wisconsin, USA, 2001.
(25) Bruker AXS Inc. *APEX5* Madison, Wisconsin, USA, 2023.
(26) Sheldrick, G. M. *SHELXT* − Integrated Space-Group and Crystal-Structure Determination. *Acta Crystallogr., Sect. A: Found. Adv.* **2015**, *A71* (1), 3−8.
(27) Sheldrick, G. M. Crystal Structure Refinement with *SHELXL*. *Acta Crystallogr., Sect. C: Struct. Chem.* **2015**, *C71* (1), 3−8.
(28) Hübschle, C. B.; Sheldrick, G. M.; Dittrich, B. *ShelXle* : A Qt Graphical User Interface for *SHELXL*. *J. Appl. Crystallogr.* **2011**, *44* (6), 1281−1284.
(29) Stoe & Cie GmbH. *WinXpow*, version 3.12, Darmstadt, Germany, 2018.
(30) Krywka, C.; Sternemann, C.; Paulus, M.; Javid, N.; Winter, R.; Al-Sawalmih, A.; Yi, S.; Raabe, D.; Tolan, M. The Small-Angle and Wide-Angle X-Ray Scattering Set-up at Beamline BL9 of DELTA. *J. Synchrotron Radiat.* **2007**, *14* (3), 244−251.
(31) Coelho, A. A. *TOPAS* and *TOPAS-Academic* : An Optimization Program Integrating Computer Algebra and Crystallographic Objects Written in C++. *J. Appl. Crystallogr.* **2018**, *51* (1), 210−218.
(32) Brandenburg, K.; Putz, H. *Diamond: Crystal and Molecular Structure Visualization*; Crystal Impact: Bonn, Germany, 2008.
(33) Tobeck, C. Analyse der gasförmigen Hydrolyseprodukte von binären und ternären Carbiden. Master Thesis; University of Cologne: Cologne, Germany, 2017.
(34) Fjellvaag, H.; Karen, P. Crystal Structure of Magnesium Sesquicarbide. *Inorg. Chem.* **1992**, *31* (15), 3260−3263.
(35) Calder, R. S.; Cochran, W.; Griffiths, D.; Lowde, R. D. An X-Ray and Neutron Diffraction Analysis of Lithium Hydride. *J. Phys. Chem. Solids* **1962**, *23* (6), 621−632.
(36) Bain, G. A.; Berry, J. F. Diamagnetic Corrections and Pascal's Constants. *J. Chem. Educ.* **2008**, *85* (4), 532−536.
(37) Long, G. J.; Cranshaw, T. E.; Longworth, G. The Ideal Mössbauer Effect Absorber Thickness. *Moessbauer Eff. Ref. Data J.* **1983**, *6*, 42−49.
(38) Brand, R. A. *WinNormos for Igor7 (Version for Igor 7.010 or above: 01/03/2020)*; University of Duisburg: Duisburg, Germany, 2020.
(39) Corel Corporation. *CorelDRAW Graphics Suite* Ottawa, Ontario, Canada, 2018.
(40) Farla, R.; Bhat, S.; Sonntag, S.; Chanyshev, A.; Ma, S.; Ishii, T.; Liu, Z.; Néri, A.; Nishiyama, N.; Faria, G. A.; Wroblewski, T.; Schulte-Schrepping, H.; Drube, W.; Seeck, O.; Katsura, T. Extreme Conditions Research Using the Large-Volume Press at the P61B Endstation, PETRA III. *J. Synchrotron Radiat.* **2022**, *29* (2), 409−423.
(41) Brown, J. M. The NaCl Pressure Standard. *J. Appl. Phys.* **1999**, *86* (10), 5801−5808.
(42) Matsui, M. Temperature−Pressure−Volume Equation of State of the B1 Phase of Sodium Chloride. *Phys. Earth Planet. Inter.* **2009**, *174* (1−4), 93−97.
(43) Seto, Y.; Nishio-Hamane, D.; Nagai, T.; Sata, N. Development of a Software Suite on X-Ray Diffraction Experiments. *Rev. High Pressure Sci. Technol.* **2010**, *20* (3), 269−276.
(44) Seto, Y. Whole Pattern Fitting for Two-Dimensional Diffraction Patterns from Polycrystalline Materials. *Rev. High Pressure Sci. Technol.* **2012**, *22* (2), 144−152.
(45) Angel, R. J.; Alvaro, M.; Gonzalez-Platas, J. EosFit7c and a Fortran Module (Library) for Equation of State Calculations. *Z. Kristallogr. Cryst. Mater.* **2014**, *229* (5), 405−419.
(46) Perdew, J. P.; Ruzsinszky, A.; Csonka, G. I.; Vydrov, O. A.; Scuseria, G. E.; Constantin, L. A.; Zhou, X.; Burke, K. Restoring the Density-Gradient Expansion for Exchange in Solids and Surfaces. *Phys. Rev. Lett.* **2008**, *100* (13), No. 136406.
(47) Giannozzi, P.; Baroni, S.; Bonini, N.; Calandra, M.; Car, R.; Cavazzoni, C.; Ceresoli, D.; Chiarotti, G. L.; Cococcioni, M.; Dabo, I.; Dal Corso, A.; de Gironcoli, S.; Fabris, S.; Fratesi, G.; Gebauer, R.; Gerstmann, U.; Gougoussis, C.; Kokalj, A.; Lazzeri, M.; Martin-Samos, L.; Marzari, N.; Mauri, F.; Mazzarello, R.; Paolini, S.; Pasquarello, A.; Paulatto, L.; Sbraccia, C.; Scandolo, S.; Sclauzero, G.; Seitsonen, A. P.; Smogunov, A.; Umari, P.; Wentzcovitch, R. M. QUANTUM ESPRESSO: A Modular and Open-Source Software Project for Quantum Simulations of Materials. *J. Phys.: Condens. Matter* **2009**, *21* (39), No. 395502.
(48) Dal Corso, A. Pseudopotentials Periodic Table: From H to Pu. *Comput. Mater. Sci.* **2014**, *95*, 337−350.
(49) Topsakal, M.; Wentzcovitch, R. M. Accurate Projected Augmented Wave (PAW) Datasets for Rare-Earth Elements (RE = La−Lu). *Comput. Mater. Sci.* **2014**, *95*, 263−270.
(50) Blöchl, P. E. Projector Augmented-Wave Method. *Phys. Rev. B* **1994**, *50* (24), No. 17953.
(51) Dronskowski, R.; Bloechl, P. E. Crystal Orbital Hamilton Populations (COHP): Energy-Resolved Visualization of Chemical Bonding in Solids Based on Density-Functional Calculations. *J. Phys. Chem. A* **1993**, *97* (33), 8617−8624.
(52) Deringer, V. L.; Tchougréeff, A. L.; Dronskowski, R. Crystal Orbital Hamilton Population (COHP) Analysis As Projected from Plane-Wave Basis Sets. *J. Phys. Chem. A* **2011**, *115* (21), 5461−5466.
(53) Maintz, S.; Deringer, V. L.; Tchougréeff, A. L.; Dronskowski, R. Analytic Projection from Plane-Wave and PAW Wavefunctions and Application to Chemical-Bonding Analysis in Solids. *J. Comput. Chem.* **2013**, *34* (29), 2557−2567.
(54) Maintz, S.; Deringer, V. L.; Tchougréeff, A. L.; Dronskowski, R. LOBSTER: A Tool to Extract Chemical Bonding from Plane-wave Based DFT. *J. Comput. Chem.* **2016**, *37* (11), 1030−1035.
(55) Nelson, R.; Ertural, C.; George, J.; Deringer, V. L.; Hautier, G.; Dronskowski, R. LOBSTER: Local orbital proections, atomic charges, and chemical-bonding analysis from projector-augmented-wave-based density-functional theory. *J. Comput. Chem.* **2020**, *41* (21), 1931−1940.
(56) Ertural, C.; Steinberg, S.; Dronskowski, R. Development of a Robust Tool to Extract Mulliken and Löwdin Charges from Plane Waves and Its Application to Solid-State Materials. *RSC Adv.* **2019**, *9* (51), 29821−29830.
(57) Müller, P. C.; Ertural, C.; Hempelmann, J.; Dronskowski, R. Crystal Orbital Bond Index: Covalent Bond Orders in Solids. *J. Phys. Chem. C* **2021**, *125* (14), 7959−7970.
(58) Müller, P. C.; Schmit, N.; Sann, L.; Steinberg, S.; Dronskowski, R. Fragment Orbitals Extracted from First-Principles Plane-Wave Calculations. *Inorg. Chem.* **2024**, *63* (43), 20161−20172.
(59) Wang, Y.; Müller, P. C.; Hemker, D.; Dronskowski, R. LOPOSTER: A Cascading Postprocessor for LOBSTER. *J. Comput. Chem.* **2025**, *46* (17), No. e70167.
(60) Racine, J. Gnuplot 4.0: A Portable Interactive Plotting Utility. *J. Appl. Econometrics* **2006**, *21* (1), 133−141.
(61) Blankenship, T. V.; Chen, B.; Latturner, S. E. $Ca_{54}In_{13}B_{4-x}H_{23+x}$: A Complex Metal Subhydride Featuring Ionic and Metallic Regions. *Chem. Mater.* **2014**, *26* (10), 3202−3208.

https://doi.org/10.1021/jacs.5c19173
J. Am. Chem. Soc. XXXX, XXX, XXX−XXX

(62) Haschke, J. M.; Clark, M. R. Phase Equilibria and Crystal Growth of Alkaline Earth and Lanthanide Dihydrides. *High Temp. Sci.* **1975**, *7* (2), 152−158.
(63) Bischof, R.; Kaldis, E.; Wachter, P. Synthesis, Crystallographic and Physical Properties of Europium Dihydride. *J. Less-Common Met.* **1985**, *111* (1−2), 139−144.
(64) Kohlmann, H.; Yvon, K. The Crystal Structures of EuH_2 and $EuLiH_3$ by Neutron Powder Diffraction. *J. Alloys Compd.* **2000**, *299* (1−2), L16−L20.
(65) Moxon, M. C.; Endacott, D. A. J.; Jolly, J. E. The Neutron Capture Cross-Section of ^{151}Eu and ^{153}Eu in the Energy Range 0.1 to 100 KeV. *Ann. Nucl. Energy* **1976**, *3* (7−8), 399−403.
(66) Gharghouri, M. A. Incoherent Neutron Scattering. In *Neutron Scattering and Other Nuclear Techniques for Hydrogen in Materials*; Springer, 2016; pp 227−244.
(67) Glazer, A. M. The Classification of Tilted Octahedra in Perovskites. *Acta Crystallogr., Sect. B: Struct. Crystallogr. Cryst. Chem.* **1972**, *28* (11), 3384−3392.
(68) Link, L.; Niewa, R. *Polynator*: A Tool to Identify and Quantitatively Evaluate Polyhedra and Other Shapes in Crystal Structures. *J. Appl. Crystallogr.* **2023**, *56* (6), 1855−1864.
(69) Pöttgen, R.; Jeitschko, W. Scandium Carbide, Sc_3C_4, a Carbide with C_3 Units Derived from Propadiene. *Inorg. Chem.* **1991**, *30* (3), 427−431.
(70) Meyer, H.-J. Darstellung und Kristallstruktur eines Calcium-carbidchlorides mit einer C_3^{4-}-Einheit, $Ca_3Cl_2C_3$. *Z. Anorg. Allg. Chem.* **1991**, *593* (1), 185−192.
(71) Pauling, L.; Brockway, L. O. Carbon—Carbon Bond Distances. The Electron Diffraction Investigation of Ethane, Propane, Isobutane, Neopentane, Cyclopropane, Cyclopentane, Cyclohexane, Allene, Ethylene, Isobutene, Tetramethylethylene, Mesitylene, and Hexamethylbenzene. Revised Values of Covalent Radii. *J. Am. Chem. Soc.* **1937**, *59* (7), 1223−1236.
(72) Ruschewitz, U.; Pöttgen, R. Structural Phase Transition in Li_2C_2. *Z. Anorg. Allg. Chem.* **1999**, *625* (10), 1599−1603.
(73) Shannon, R. D. Revised Effective Ionic Radii and Systematic Studies of Interatomic Distances in Halides and Chalcogenides. *Acta Crystallogr., Sect. A* **1976**, *32* (5), 751−767.
(74) Bärnighausen, H. Group-Subgroup Relations between Space Groups: A Useful Tool in Crystal Chemistry. *MATCH Commun. Math. Chem.* **1980**, *9*, 139−175.
(75) Stokes, H. T.; Hatch, D. M.; Campbell, B. J. ISODISTORT, ISOTROPY Software Suite, iso.byu.edu..
(76) Campbell, B. J.; Stokes, H. T.; Tanner, D. E.; Hatch, D. M. *ISODISPLACE*: A Web-Based Tool for Exploring Structural Distortions. *J. Appl. Crystallogr.* **2006**, *39* (4), 607−614.
(77) Pöttgen, R. Coloring, Distortions, and Puckering in Selected Intermetallic Structures from the Perspective of Group-Subgroup Relations. *Z. Anorg. Allg. Chem.* **2014**, *640* (5), 869−891.
(78) Reimann, M. K.; Kösters, J.; Bieliauskas, T.; Pöttgen, R. The Crystal Structures of the Ternary Intermetallics RE_2Pd_2Cd (*RE* = Nd, Sm, Gd, Dy) and RE_2Ga_2Mg (*RE* = Tb, Er, Tm, Lu) at 90 K. *Z. Naturforsch., B* **2024**, *79* (5−6), 349−355.
(79) Peterson, G. G. C.; Hilleke, K. P.; Lotfi, S.; Wang, F.; Zurek, E.; Brgoch, J. Twists and Puckers: Tuning Crystal Chemistry in the $La(Au_xGe_{1-x})_2$ Compositional Series. *J. Am. Chem. Soc.* **2023**, *145* (39), 21612−21622.
(80) Buerger, M. J. Polymorphism and Phase Transformations. *Fortschr. Mineral.* **1961**, *39*, 9−24.
(81) Landau, L. D. On the Theory of Phase Transitions. *Zh. Eksp. Teor. Fiz.* **1937**, *7*, 19−32.
(82) Cordes, J. F.; Wintersberger, K. Notizen: Zur Struktur des Mg_2C_3. *Z. Naturforsch., B* **1957**, *12* (2), 136−137.
(83) Holleck, H. The Effect of Carbon on the Occurrence of Cu_3Au-type Phases in Actinide-and Lanthanide-Platinum Metal Systems. *J. Nucl. Mater.* **1972**, *42* (3), 278−284.
(84) Larson, J. T.; Wix, K. D.; Chen, B.; Latturner, S. E. Metal Flux Growth Of Lanthanide Carbide Hydrides Using Anthracene. *Inorg. Chem.* **2023**, *62* (33), 13277−13283.
(85) Bischof, R.; Kaldis, E.; Wachter, P. EuH_2: A New Ferromagnetic Semiconductor. *J. Magn. Magn. Mater.* **1983**, *31*−*34* (1), 255−256.
(86) Pöttgen, R.; Johrendt, D. Equiatomic Intermetallic Europium Compounds: Syntheses, Crystal Chemistry, Chemical Bonding, and Physical Properties. *Chem. Mater.* **2000**, *12* (4), 875−897.
(87) Chien, C.-L.; Greedan, J. E. A Study of the Spontaneous Magnetization of $EuLiH_3$ Using the Mössbauer Effect. *Phys. Lett. A* **1971**, *36* (3), 197−198.
(88) Gerth, G.; Kienle, P.; Luchner, K. Chemical Effects on the Isomer Shift in ^{151}Eu. *Phys. Lett. A* **1968**, *27* (8), 557−558.
(89) Cunningham, G. W. Nuclear Poisons. *React. Mater.* **1963**, *6*, 63−66.
(90) Jayaraman, A. Pressure-Induced Electronic Collapse and Semiconductor-to-Metal Transition in EuO. *Phys. Rev. Lett.* **1972**, *29* (25), No. 1674.
(91) Xu, M.; Jose, G. C.; Cheng, M.; Peng, C.; Gonzalez Jimenez, J. L.; Bi, W.; Li, M.; Xie, W. Continuous Evolution of Eu^{2+}/Eu^{3+} Mixed Valency Driven by Pressure and Temperature. *J. Phys. Chem. A* **2025**, *129* (9), 2371−2377.
(92) Berman, R. G. Internally-Consistent Thermodynamic Data for Minerals in the System Na_2O-K_2O-CaO-MgO-FeO-Fe_2O_3-Al_2O_3-SiO_2-TiO_2-H_2O-CO_2. *J. Petrol.* **1988**, *29* (2), 445−522.
(93) Touloukian, Y. S.; Kirby, R. K.; Taylor, R. E.; Desai, P. D. *Thermophysical Properties of Matter - the TPRC Data Series. Vol. 12. Thermal Expansion Metallic Elements and Alloys*; Defense Technical Information Center, 1975.
(94) Engel, S.; Gießelmann, E. C. J.; Pöttgen, R.; Janka, O. Trivalent Europium − a Scarce Case in Intermetallics. *Rev. Inorg. Chem.* **2023**, *43* (4), 571−582.
(95) Neziraj, T.; Akselrud, L.; Schmidt, M.; Burkhardt, U.; Grin, Y.; Schwarz, U. Locating Hydrogen in the $Mg_5Bi_3H_x$ Zintl Phase. *Commun. Chem.* **2025**, *8* (1), No. 132.

https://doi.org/10.1021/jacs.5c19173
J. Am. Chem. Soc. XXXX, XXX, XXX−XXX